Bulk and surface properties in the critical phase of the two-dimensional *XY* model

Bulk and surface properties in the critical phase of the two-dimensional *XY* model*

Bertrand Berche

Laboratoire de Physique des Matériaux, Université Henri Poincaré, Nancy 1, BP 239,
F-54506 Vandœuvre les Nancy, France

E-mail: berche@lpm.u-nancy.fr

Abstract
Monte Carlo simulations of the two-dimensional *XY* model are performed in
a square geometry with various boundary conditions (BC). Using conformal
mappings we deduce the exponent $\eta_\sigma(T)$ of the order parameter correlation
function and its surface analogue $\eta_\parallel(T)$ as a function of the temperature in the
critical (low-temperature) phase of the model. The temperature dependence
of both exponents is obtained numerically with a good accuracy up to the
Kosterlitz–Thouless transition temperature. The bulk exponent follows from
simulations of correlation functions with periodic boundary conditions or order
parameter profiles with open boundary conditions and with symmetry breaking
surface fields. At very low temperatures, $\eta_\sigma(T)$ is found in pretty good
agreement with the linear temperature-dependence of Berezinskii's spin-wave
approximation. We also show some evidence that there are no noticeable
logarithmic corrections to the behaviour of the order parameter density profile
at the Kosterlitz–Thouless (KT) transition temperature, while these corrections
exist for the correlation function. At the KT transition the value $\eta_\sigma(T_{\rm KT}) = 1/4$
is accurately recovered. The exponent associated with the surface correlations
is similarly obtained after a slight modification of the boundary conditions:
the correlation function is computed with free BC, and the profile with mixed
fixed–free BC. It exhibits a monotonic behaviour with temperature, starting
linearly according to the spin-wave approximation and increasing up to a value
$\eta_\parallel(T_{\rm KT}) \simeq 1/2$ at the Kosterlitz–Thouless transition temperature. The thermal
exponent $\eta_\varepsilon(T)$ is also computed and we give some evidence that it keeps a
constant value in agreement with the marginality condition of the temperature
field below the KT transition.

PACS numbers: 05.20.−y, 05.40.+j, 64.60.Cn, 64.60.Fr

1. Introduction

The two-dimensional classical *XY* model has a rich variety of applications in condensed matter physics [1]. It describes of course magnetic films with planar anisotropy[1], but also thin-film superfluids or superconductors, or two-dimensional solids. In statistical physics, this model was also extensively studied for fundamental reasons, as describing, for example, classical Coulomb gas or fluctuating surfaces and the roughness transition. Although no exact solution exists for this model, many of its essential properties are known from different approaches.

The model undergoes a standard temperature-driven paramagnetic to ferromagnetic phase transition in $d > 2$, characterized, e.g., by a power-law divergence of the correlation length near criticality,

$$\xi \sim |t|^{-\nu} \tag{1}$$

(see, e.g., [2]). In two dimensions, it exhibits a rather different behaviour, since long-range order of spins with continuous symmetries (if there is no source of anisotropy in spin space) is forbidden according to the Mermin–Wagner theorem [3, 4]. Indeed, there is no spontaneous magnetization at finite temperature in two-dimensional systems having a continuous symmetry group, for example *XY* or $O(2)$ spin models, since order would otherwise be destroyed by spin-wave excitations [5]. On the other hand, there is an infinite susceptibility at low temperatures, indicating another type of transition [6]. Such systems can indeed display a low-temperature phase with quasi-long-range order and a defect-mediated transition towards the usual paramagnetic phase at high temperatures. This transition is governed by unbinding of topological defects.

We now specify the case of the 2d *XY* model: consider a square lattice with two-component spin variables $\boldsymbol{\sigma}_w = (\cos\theta_w, \sin\theta_w)$, $|\boldsymbol{\sigma}_w|^2 = 1$, located at the sites w of a lattice Λ of linear extent L, and interacting through the usual nearest-neighbour ferromagnetic interaction

$$
\begin{aligned}
-\frac{H}{k_B T} &= K \sum_w \sum_\mu \boldsymbol{\sigma}_w \cdot \boldsymbol{\sigma}_{w+\hat{\mu}} \\
&= K \sum_w \sum_\mu \cos(\theta_w - \theta_{w+\hat{\mu}})
\end{aligned}
\tag{2}
$$

where $K = J/k_B T$, with J the ferromagnetic coupling strength and $\mu = 1, 2$ labels the directions in Λ ($\hat{\mu}$ is the corresponding unit vector). The angle θ_w measures the deviation of $\boldsymbol{\sigma}_w$ from an arbitrary reference direction.

The low-temperature regime, governed by spin-wave excitations, was investigated by Berezinskii [5] in the harmonic approximation. In the low-temperature limit (also called spin-wave phase), localized non-linear excitations (called vortices) are indeed bounded in pairs of zero vorticity, and thus do not affect crucially the spin-wave description. At a first approximation, the effect of vortices can be completely neglected and the spin-wave approximation, after expanding the cosine, reproduces the main features of the low-temperature physics. This harmonic approximation is justified, provided that the spin disorientation remains small, i.e. at sufficiently low temperature:

$$-\frac{H}{k_B T} \simeq -\frac{H_0}{k_B T} - \frac{1}{2} K \sum_w \sum_\mu (\theta_w - \theta_{w+\hat{\mu}})^2. \tag{3}$$

Within this approximation, the quadratic energy corresponds to a Gaussian equilibrium distribution and the two-point correlation function at inverse temperature β becomes [7–10]

---

[1] 2d *XY*-type singularities are extremely hard to observe experimentally in real magnetic layers, since they are washed out by crossover effects as soon as a small interlayer interaction takes place in the system.

$$Z_\beta = \left(\prod_w \int \frac{d\theta_w}{2\pi} \right) \prod_{w,\mu} \exp\left[-\frac{1}{2} K (\theta_w - \theta_{w+\hat\mu})^2 \right] \qquad (4)$$

$$\langle \boldsymbol{\sigma}_{w_1} \cdot \boldsymbol{\sigma}_{w_2} \rangle \simeq Z_\beta^{-1} \prod_w \int \frac{d\theta_w}{2\pi} \cos\left(\theta_{w_1} - \theta_{w_2} \right) \times \exp\left(-\frac{1}{2} K \sum_w \sum_\mu (\theta_w - \theta_{w+\hat\mu})^2 \right)$$

$$\simeq \exp\left(\left(-\frac{1}{2} Z_\beta^{-1} \prod_w \int \frac{d\theta_w}{2\pi} \left(\theta_{w_1} - \theta_{w_2} \right)^2 \right) \times \exp\left(-\frac{1}{2} K \sum_w \sum_\mu (\theta_w - \theta_{w+\hat\mu})^2 \right) \right)$$

$$\simeq |w_1 - w_2|^{-1/2\pi K} \qquad (5)$$

hence

$$\eta_\sigma^{SW}(T) = \frac{1}{2\pi K} = \frac{k_B T}{2\pi J}. \qquad (6)$$

When the temperature increases, the bounded vortices appear in increasing number. Their influence becomes more prominent, producing a deviation from the linear spin-wave contribution in equation (6), but the order parameter correlation function still decays algebraically with an exponent $\eta_\sigma(T)$ which depends on the temperature. The transition eventually takes place at a temperature T_{KT} (usually called Berezinskii–Kosterlitz–Thouless critical temperature) when the pairs dissociate, thereby destroying short-range order in the system. The mechanism of unbinding of vortices was studied by Kosterlitz and Thouless [11–13] using approximate renormalization group methods. Above T_{KT} (in the vortex phase), the correlation function recovers the usual exponential decay. This very peculiar topological transition is characterized by essential singularities when approaching the critical point from the high-temperature phase, $t = T - T_{KT} \to 0^+$,

$$\xi \sim e^{b_\xi t^{-\sigma}} \qquad (7)$$

$$\chi \sim e^{b_\chi t^{-\sigma}} \sim \xi^{2-\eta_\sigma} \qquad (8)$$

whence $\eta_\sigma \equiv \eta_\sigma(T_{KT}) = 2 - b_\chi / b_\xi$. For reviews, see e.g. [1, 14–17].

The existence of a scale-invariant power-law decay of the correlation function implies that at each value of the temperature there corresponds a fixed point, or equivalently that there is a continuous line of fixed points at low temperatures. The temperature is thus a marginal field in the spin-wave phase which becomes relevant in the vortex phase.

Not much is known in the intermediate regime between the spin-wave approximation at low temperature and the Kosterlitz–Thouless results at the topological transition and in fact the precise determination of the critical behaviour of the two-dimensional *XY* model in the critical phase remains a challenging problem. Most of the studies were dedicated to the determination of critical properties at T_{KT}.[2] Many results were obtained using Monte Carlo simulations (see, e.g., [18–29]) at T_{KT} and slightly above, or high-temperature series expansions [30, 31], but the analysis was made difficult by the existence of logarithmic corrections, e.g.

$$\chi \sim \xi^{2-\eta_\sigma} (\ln\xi)^{2\theta} \left[1 + O\left(\frac{\ln\ln\xi}{\ln\xi} \right) \right] \qquad (9)$$

in the high-temperature regime, or

$$\langle \boldsymbol{\sigma}_{w_1} \cdot \boldsymbol{\sigma}_{w_2} \rangle \simeq \frac{(\ln|w_1 - w_2|)^{2\theta}}{|w_1 - w_2|^{\eta_\sigma}} \left[1 + O\left(\frac{\ln\ln|w_1 - w_2|}{\ln|w_1 - w_2|} \right) \right] \qquad (10)$$

[2] When approaching the transition from above, the value of T_{KT} is often obtained by fixing $\sigma = 1/2$ in equation (7), and $\eta_\sigma(T_{KT})$ then follows from a fit of the susceptibility to equation (8).

at T_{KT} exactly [15, 32, 33], with a probable value of $\theta = \frac{1}{16}$ [34]. Due to these logarithmic corrections which make the fits quite difficult to achieve safely, the values of T_{KT} and $\eta_\sigma(T_{\mathrm{KT}})$ were a bit controversial as shown in table 1 of [29]. Resorting to large-scale simulations was then needed in order to confirm this picture [28]. Although essentially dedicated to the KT point, some of these papers also report the value of $\eta_\sigma(T)$ computed from the correlation function decay at several temperatures in the critical phase [18, 21–23], while a systematic study of the helicity modulus at low temperature previously led more directly to the same information [35].

Recently, we proposed a rather different approach [36, 37] which only requires a moderate computation effort. Assuming that the low-temperature phase exhibits all the characteristics of a critical phase with conformal invariance [38] (invariance under rotation, translation and scale transformations, short-range interactions, isotropic scaling), we use the covariance law of n-point correlation functions under the mapping of a two-dimensional system confined inside a square onto the infinite or half-infinite plane. The scaling dimensions are then obtained through a simple power-law fit where the shape effects are encoded in the conformal mapping, via the definition of a rescaled distance variable adapted to the description of the confined geometry.

This technique is well known since the appearance of conformal invariance. Conformal mappings have been extensively used, mainly in the case of Ising or Potts models, in order to investigate the critical properties in restricted geometries. Density profiles or correlations have been investigated in various confined systems (surfaces [39, 40], corners [41, 42], strips [43–46], squares [47, 48] or parabolic shapes [49–51]: for a review, see [52]). The exact expressions of the two-point correlation functions have also been calculated on the torus for the pure Ising case [53], and large-scale Monte Carlo simulations of the 2d Ising model have been shown to reproduce the correct behaviour, including corrections due to the finite size of the lattice [54, 55].

In this paper, we report a systematic application of conformal mappings to the investigation of critical properties of the 2d XY model in the spin-wave phase. The physical quantities are obtained using Monte Carlo simulations in square-shaped confined systems. We may then determine accurately the correlation function exponent $\eta_\sigma(T)$ in the low-temperature phase $T \leqslant T_{\mathrm{KT}}$ [36], but also, by choosing convenient boundary conditions (BC), the surface critical exponent which describes the decay of the correlation function parallel to a free surface, $\eta_\|(T)$ [37]. The thermal exponent η_ε will also be considered. Section 2 presents the expected functional expressions of correlation functions and density profiles with various BC, and use of these expressions is systematically reported in section 3. It is worth noting already that the results following the analysis of the two-point correlation functions are not fully convincing, but the main conclusions are then supported by the most refined investigations of the density profiles. A discussion of the results is given in the last section.

2. Functional expressions of correlation functions and density profiles in a square-shaped critical system

2.1. Preliminary and notation

In the following, we shall specify two different types of geometries, depending on our purpose. They are related through a conformal transformation. The critical properties in the first system will be reached through the study of the confined system in the second one.

(i) The infinite plane

$$z = x + \mathrm{i}y \qquad -\infty < \mathrm{Re}\, z < +\infty \qquad -\infty < \mathrm{Im}\, z < +\infty \qquad (11)$$

or the upper half-plane

$$z = x + \mathrm{i}y \qquad -\infty < \mathrm{Re}\, z < +\infty \qquad y = \mathrm{Im}\, z \geqslant 0. \tag{12}$$

This is the system which is eventually interesting in the thermodynamic limit. It is of course not directly accessible using numerical techniques. In the second case, the existence of a free surface materialized here by the real axis will allow us to define both bulk and surface quantities.

(ii) The square

$$w = u + \mathrm{i}v \qquad -L/2 \leqslant \mathrm{Re}\, w \leqslant L/2 \qquad 0 \leqslant \mathrm{Im}\, w \leqslant L. \tag{13}$$

This is the natural geometry for Monte Carlo simulations. The boundary conditions may be open at the edges (square) or periodic (torus). In the following, we will obtain numerical results in the square or the torus, and our aim will be to translate them into their half-infinite or infinite system counterpart[3].

It is worth referring also to the infinitely long strip of width L, $k+\mathrm{i}l$, $-\infty < k < +\infty$, $0 \leqslant l \leqslant L$: this geometry is incidentally mentioned here because the choice of the boundary conditions is more obvious there than in the square system. Although no computation will be performed in this geometry, we will refer to it when introducing the profiles. It is particularly interesting, since many results concern such strips, e.g. when obtained with transfer matrices [56] or quantum chains [57] which correspond to the Hamiltonian limit of classical systems confined in strips. In the transverse direction (l-coordinate), the boundary conditions may be open (strip) or periodic (cylinder). A very accurate numerical study of the $O(n)$ model (including XY) using the transfer matrix of a related loop gas model was, for example, reported by Blöte and Nienhuis [56]. The periodic strip is obtained from the plane through the standard logarithmic mapping $k + \mathrm{i}l = \frac{L}{2\pi} \ln z$ which implies an asymptotic exponential decay for the correlation functions along the strip at criticality,

$$\left\langle \boldsymbol{\sigma}_{k_1+\mathrm{i}l} \boldsymbol{\sigma}_{k_2+\mathrm{i}l} \right\rangle_{\text{PBC}} \sim \exp(-2\pi x_\sigma |k_1 - k_2|/L). \tag{14}$$

The scaling dimensions are thus determined by the universal correlation length amplitudes, $\xi_\sigma^{-1} = 2\pi x_\sigma/L$, which are given, in the transfer matrix formalism, by the two leading eigenvalues of the transfer matrix $\xi_\sigma^{-1} = \ln(\Lambda_0/\Lambda_1)$. Blöte and Nienhuis obtained the most precise values of the thermal and magnetic scaling dimensions at the KT transition, $x_\varepsilon = \frac{1}{2}\eta_\varepsilon = 2.000\,000\,(2)$ and $x_\sigma = \frac{1}{2}\eta_\sigma = 0.125\,000\,(1)$. In the following, we will exploit expressions similar to equation (14), transposed in the square geometry. We mention here that our approach proceeds from Monte Carlo simulations and cannot pretend to an accuracy comparable to the results of Blöte and Nienhuis.

2.2. Conformal rescaling of the correlation functions

In an infinite system at criticality, the correlation function is known to behave asymptotically as

$$\left\langle \boldsymbol{\sigma}_{z_1} \cdot \boldsymbol{\sigma}_{z_2} \right\rangle \sim |z_1 - z_2|^{-\eta_\sigma}. \tag{15}$$

This defines the bulk correlation function exponent η_σ. The surface critical properties are also interesting and extra universal critical exponents can be measured from simulations performed in finite systems with open boundary conditions. In the semi-infinite geometry $z = x + \mathrm{i}y$

---

[3] Here and in the following, z will constantly refer to a complex coordinate in the plane, while w will refer to the complex coordinate in the square geometry. In the plane, UHP specifies the upper half-plane. In the square, PBC, FBC, FBC and FfBC mean that the boundary conditions are respectively periodic, free, fixed, or mixed fixed–free according to a description which will be given later.

(the free surface being defined by the x-axis), the two-point correlation function is fixed up to an unknown scaling function. Fixing one point z_1 close to the free surface ($z_1 = i$) of the upper half-plane (UHP), and leaving the second point z_2 to explore the rest of the geometry, the following behaviour is expected:

$$\left\langle \boldsymbol{\sigma}_{z_1} \cdot \boldsymbol{\sigma}_{z_2} \right\rangle_{\text{UHP}} \sim (y_1 y_2)^{-x_\sigma} \psi(\omega) \tag{16}$$

with $\eta_\sigma = 2x_\sigma$. The dependence on

$$\omega = \frac{y_1 y_2}{|z_1 - z_2|^2} \tag{17}$$

of the universal scaling function ψ is constrained by the special conformal transformation [39, 40], and its asymptotic behaviour is implied by scaling, e.g. $\psi(\omega) \sim \omega^{x_\sigma^1}$ when $y_2 \gg 1$, with $x_\sigma^1 = \frac{1}{2} \eta_\parallel$ the magnetic surface scaling dimension.

In a square system, the order parameter correlation function $\left\langle \boldsymbol{\sigma}_{w_1} \cdot \boldsymbol{\sigma}_{w_2} \right\rangle$ is strongly affected by boundary and shape effects and thus deviates significantly from the thermodynamic limit expressions (15) and (16). It should obey a scaling form which reproduces the expected power-law behaviour, for example,

$$\left\langle \boldsymbol{\sigma}_{w_1} \cdot \boldsymbol{\sigma}_{w_2} \right\rangle = |w_1 - w_2|^{-\eta_\sigma} f_{\text{sq}}(w_1/L, w_2/L) \tag{18}$$

where the function f_{sq} encodes shape effects in a very complicated manner which also depends on the boundary conditions so that the connection between equations (15) or (16) and (18) is not obvious. Conformal invariance provides an efficient technique to avoid these shape effects, or at least, enable us to include explicitly the shape dependence in the functional expression of the correlators through the conformal covariance transformation under a mapping $w(z)$:

$$\left\langle \boldsymbol{\sigma}_{w_1} \cdot \boldsymbol{\sigma}_{w_2} \right\rangle = |w'(z_1)|^{-x_\sigma} |w'(z_2)|^{-x_\sigma} \left\langle \boldsymbol{\sigma}_{z_1} \cdot \boldsymbol{\sigma}_{z_2} \right\rangle. \tag{19}$$

Conformal invariance holds in isotropic systems with short-range interactions which exhibit translation, rotation, as well as scale invariance. Usually, these conditions are so restrictive that they can only be valid at the critical point, and we assume here that the general covariance equation (19) holds in the whole $T < T_{\text{KT}}$ phase.

In order to get a functional expression of the correlation function inside the square geometry w, one simply has to use the convenient mapping $w(z)$:

(i) *Conformal mapping of the plane onto the torus:* in the continuum limit, the correlation function of the Ising model on the torus is exactly known [40, 53, 58]

$$\left\langle \boldsymbol{\sigma}_{w_1} \cdot \boldsymbol{\sigma}_{w_2} \right\rangle_{\text{PBC Ising}} \sim \left[\sum_{\nu=2}^{4} |\theta_\nu(0)| \right]^{-1} \sum_{\nu=1}^{4} \left| \theta_\nu \left(\frac{w_{12}}{2L} \right) \right| \times \left| \theta_1'(0)/\theta_1 \left(\frac{w_{12}}{L} \right) \right|^{1/4} \tag{20}$$

($\eta_\sigma = 1/4$) where $\theta_\nu(\alpha)$ are the Jacobi theta functions and $w_{12} = w_1 - w_2$. A similar expression exists for the energy–energy correlations [40]. It can be generalized to a critical system characterized by any correlation function exponent η_σ. For simplicity, we fix in the following one point (w_1) as the origin, and the second point is simply written as w. The dependence on the relative distance w in the above expression,

$$\left\langle \boldsymbol{\sigma}_0 \cdot \boldsymbol{\sigma}_w \right\rangle_{\text{PBC}} \sim \sum_{\nu=1}^{4} |\theta_\nu(w/2L)| \times |\theta_1(w/L)|^{-1/4} \tag{21}$$

is compatible with the general covariance equation (19), rewritten as

$$\left\langle \boldsymbol{\sigma}_0 \cdot \boldsymbol{\sigma}_w \right\rangle_{\text{PBC}} \sim |w'(z)|^{-\eta_\sigma/2} [z(w)]^{-\eta_\sigma} \tag{22}$$
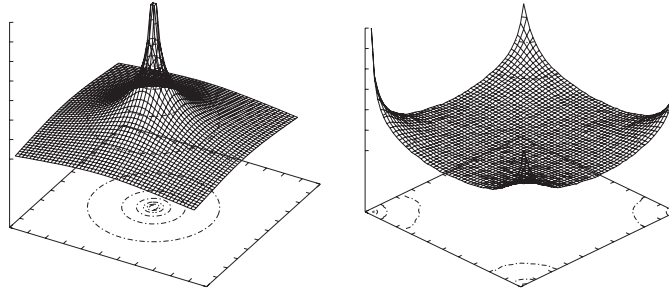
Figure 1. Correlation functions in the plane (left) and in the square (PBC) geometries (right).

provided that $|z(0)| \ll |z(w)|$ (large-distance behaviour). The rhs is a function of w hereafter denoted by $[\zeta(w)]^{-\eta_\sigma}$, with $\eta_\sigma = 1/4$ and the rescaled distance is

$$\zeta(w) = |\theta_1(w/L)| \times \left(\sum_{\nu=1}^{4} |\theta_\nu(w/2L)| \right)^{-4}. \tag{23}$$

Therefore equation (20) can be generalized to any correlation function of a critical system inside a torus,

$$\langle \boldsymbol{\sigma}_0 \cdot \boldsymbol{\sigma}_w \rangle_{\text{PBC}} \sim [\zeta(w)]^{-\eta_\sigma}. \tag{24}$$

A sketch of the correlation functions in the plane and in the square geometries is shown in figure 1.

(ii) *Conformal rescaling of the upper half-plane inside a square:* the conformal transformation of the half-plane $z = x + \mathrm{i}y$ ($0 \leqslant y < \infty$) inside a square $w = u + \mathrm{i}v$ of size $L \times L$ ($-L/2 \leqslant u \leqslant L/2, 0 \leqslant v \leqslant L$) with open boundary conditions along the four edges is realized by a Schwarz–Christoffel transformation [59]

$$w(z) = \frac{L}{2K} F(z, k) \qquad z = \mathrm{sn}\left(\frac{2Kw}{L} \right). \tag{25}$$

Here, $F(z, k)$ is the elliptic integral of the first kind,

$$F(z, k) = \int_0^z [(1 - t^2)(1 - k^2 t^2)]^{-1/2} \, \mathrm{d}t \tag{26}$$

$\mathrm{sn}(2Kw/L)$ the Jacobian elliptic sine, $K = K(k) = F(1, k)$ the complete elliptic integral of the first kind and the modulus k depends on the aspect ratio of Λ and is here the solution of $K(k)/K(\sqrt{1 - k^2}) = \frac{1}{2}$:

$$k = 4 \left(\frac{\sum_{p=0}^{\infty} q^{(p+1/2)^2}}{1 + 2 \sum_{p=1}^{\infty} q^{p^2}} \right)^2 \simeq 0.171\,573 \qquad q = \mathrm{e}^{-2\pi}. \tag{27}$$

Using mapping (25), one obtains the local rescaling factor in equation (19), $w'(z) = \frac{L}{2K}[(1 - z^2)(1 - k^2 z^2)]^{-1/2}$, and inside the square, keeping $w_1 \sim O(1)$ fixed, the two-point correlation function becomes (see, e.g., [60])

$$\langle \boldsymbol{\sigma}_0 \cdot \boldsymbol{\sigma}_w \rangle_{\text{fBC}} \sim [\kappa(w)]^{-\frac{1}{2}\eta_\sigma} \psi(\omega)$$

$$\kappa(w) = \mathrm{Im}\left[\mathrm{sn}\frac{2Kw}{L} \right] \times \left| \left(1 - \mathrm{sn}^2\frac{2Kw}{L} \right) \left(1 - k^2 \mathrm{sn}^2\frac{2Kw}{L} \right) \right|^{-1/2} \tag{28}$$

provided that $y(0) \ll y(w)$ and where fBC specifies that the open square has free boundary conditions. This expression is correct up to a constant amplitude determined by $\kappa(w_1)$
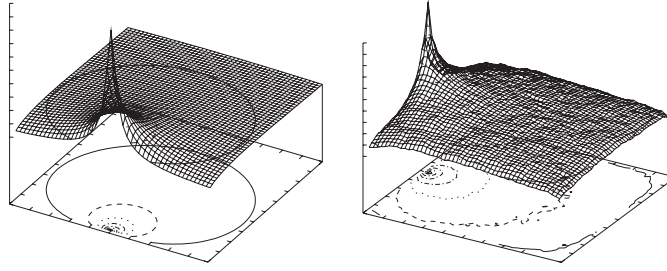
Figure 2. Correlation functions in the upper half-plane (left) and in the square (fBC) geometries (right).

which is kept fixed, but the function $\psi(\omega)$ is still varying with the location of the second point, w.

A sketch of the correlation functions in the plane and square geometries is shown in figure 2.

2.3. Density profiles in restricted geometries

In order to cancel the role of the unknown scaling function in the half-plane geometry in equation (28), it is more convenient to work with a density profile $m(w)$ in the presence of symmetry breaking surface fields $\mathbf{h}_{\partial\Lambda}$ on the boundary $\partial\Lambda$ of the lattice Λ. This is a one-point correlator which scales in the half-infinite geometry as

$$m(z) = \langle \boldsymbol{\sigma}_z \cdot \mathbf{h}_{\partial\Lambda(z)} \rangle_{\text{UHP}} = \text{const} \times y^{-x_\sigma} \tag{29}$$

and it maps onto (see figure 3)

$$m_{\text{FBC}}(w) = \langle \boldsymbol{\sigma}_w \cdot \mathbf{h}_{\partial\Lambda(w)} \rangle_{\text{FBC}} = \text{const} \times [\kappa(w)]^{-\frac{1}{2}\eta_\sigma} \tag{30}$$

where the function $\kappa(w)$ defined in equation (28) again comes from the mapping and FBC means that the open square has fixed boundary conditions (figure 3).

Equation (29) is a special case of conformally invariant profiles predicted, e.g., by Burkhardt and Xue [44, 45] in strip geometries $k + il$ or in their half-infinite counterpart $z = x + iy$:

$$m_{ab}(z) = y^{-x_\sigma} F_{ab}(\cos\theta). \tag{31}$$

The scaling function $F_{ab}(x)$ depends on the universality class and on the boundary conditions denoted by a and b [61]. This notation is reminiscent of the strip geometry where a and b specify the two boundaries of the strip at $l = 0$ and $l = L$, respectively. In the case of fixed BC (denoted by FBC in the square and FF in the strip) corresponding to equations (29) and (30), one gets

$$m_{\text{FBC}}(z) = y^{-\eta_\sigma/2} \tag{32}$$

while in the case of fixed–free BC (FfBC in the square or more naturally Ff in the strip)[4] Burkhardt and Xue have shown in the case of Ising and Potts models that

$$m_{\text{FfBC}}(z) = y^{-\eta_\sigma/2} \left(\cos\tfrac{1}{2}\theta \right)^{\eta_\parallel/2}. \tag{33}$$

---

[4] The spins located on the $x > 0$ half-axis ($l = 0$ strip surface) are kept fixed while those of the $x < 0$ half-axis ($l = L$ strip surface) are free.
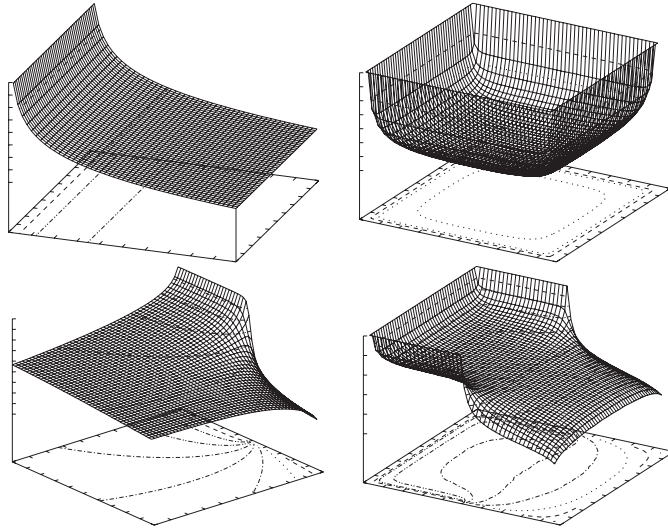
Figure 3. Order parameter profile in the plane (left) and in the square geometries (right) with fixed BC (top) and mixed fixed–free BC (bottom).

This expression has since then mainly been used in the strip geometry [62][5]. In the square geometry, the fixed–free BC correspond to keeping the spins fixed for $u > 0$, and the profile is expected to obey the following ansatz [37] (figure 3):

$$m_{\text{FfBC}}(w) \sim \text{const} \times [\kappa(w)]^{-\frac{1}{2}\eta_\sigma} [\mu(w)]^{\frac{1}{2}\eta_\parallel}$$

$$\mu(w) = \frac{1}{\sqrt{2}} \left(1 + \text{Re}\left[\text{sn}\frac{2\text{K}w}{L} \right] \times \left| \text{sn}\frac{2\text{K}w}{L} \right|^{-1} \right)^{1/2}.$$

(34)

In this paper we will essentially apply equations (24), (28), (30) and (34) in order to determine η_σ and $\eta_\parallel$.

3. Monte Carlo simulations

3.1. Description of the algorithm

Simulations of 2d *XY* spins are performed using Wolff's cluster Monte Carlo algorithm [63]. The boundary conditions may be periodic, free or fixed. When the boundaries are left periodic or free, there is no particular problem, but a relatively precise numerical determination of the order parameter profile of the 2d *XY* model confined inside a square with fixed boundary conditions (playing the role of ordering surface fields $\mathbf{h}_{\partial \Lambda(w)}$) introduces *a priori* a technical difficulty which is easily circumvented. In practice, the symmetry is broken by keeping the boundary spins located along the four edges of the square fixed, e.g. $\boldsymbol{\sigma}_w = (1, 0)$, $\forall w \in \partial \Lambda$ during the Monte Carlo simulation. The Wolff algorithm should thus become less efficient, since close to criticality the unique cluster will often reach the boundary and no update would be made in this case. To prevent this, we use the symmetry of the Hamiltonian (2) under a

---

[5] Considering a semi-infinite system described by $z = x + \mathrm{i}y = R\mathrm{e}^{\mathrm{i}\theta}$, $y \geqslant 0$, ordinary scaling implies a functional form in the half-plane, $m(z) = y^{-x_\sigma} F_{ab}(x/R)$. Under the logarithmic transformation into a strip of width L, $\frac{L}{\pi} \ln z = k + \mathrm{i}l$, one obtains the order parameter profile as $m(l) = [\frac{L}{\pi} \sin(\pi \frac{l}{L})]^{-x_\sigma} F_{ab}(\frac{\pi l}{L})$.

global rotation of all the spins. Even when the cluster reaches the fixed boundaries $\partial\Lambda(w)$, it is updated, and the order parameter profile is then measured with respect to the common new direction of the boundary spins, $m_{\text{FBC}}(w) = \langle\boldsymbol{\sigma}_w \cdot \boldsymbol{\sigma}_{\partial\Lambda(w)}\rangle_{\text{FBC}}$. The new configuration reached would thus correspond—after a global rotation of all the spins of the system to re-align the boundary spins in their original $(1, 0)$ direction—to a new configuration of equal total energy and thus the same statistical weight as the one actually produced.

In the literature, many papers were dedicated to the study of the characteristic properties of the Kosterlitz–Thouless transition. The value of T_{KT} will be considered as known with a good accuracy[6]. We will take here the value reported by Gupta and Baillie [23], or Campostrini *et al* [34], $k_B T_{\text{KT}}/J = 0.893(1)$.

3.2. Behaviour of the correlation functions

3.2.1. Scaling of $\langle\boldsymbol{\sigma}_0\cdot\boldsymbol{\sigma}_w\rangle_{\text{PBC}}$. Simulations are performed on a square with periodic boundary conditions. Here we choose systems of size $L = 100$. After thermalization (10^6 iterations) and computation (10^6 other iterations), we get the spin orientations $\{\theta_w\}$ at all the lattice sites. The correlation function is defined as

$$\langle\boldsymbol{\sigma}_0 \cdot \boldsymbol{\sigma}_w\rangle_{\text{PBC}} = \langle\cos(\theta_0 - \theta_w)\rangle_{\text{PBC}} \tag{35}$$

where 0 is an arbitrary reference site (e.g. a corner in figure 1).

It has to be fitted to equation (24) with $\zeta(w)$ given by equation (23). Expansions of the θ-functions can be found in the literature, e.g. in Abramowitz and Stegun [64],

$$\theta_1(w/L) = 2e^{-\pi/4}\sum_{n=0}^{\infty}(-1)^n e^{-n(n+1)\pi}\sin\left[\frac{(2n+1)\pi w}{L}\right] \tag{36}$$

and similar expressions for θ_2, θ_3 and θ_4. Here the fact that the system is inside a square (not a rectangle $L \times L'$) has been taken into account, therefore the expansion parameter $e^{-\pi L'/L}$ reduces to $q = e^{-\pi}$. Keeping only the leading terms, we obtain

$$\theta_1(w/L) = 2e^{-\pi/4}(\sin\pi w/L - e^{-2\pi}\sin 3\pi w/L + \cdots) \tag{37}$$

$$\sum_{\nu=1}^{4}|\theta_\nu(w/2L)| = 2(1 + e^{-\pi/4}(\sin\pi w/2L + \cos\pi w/2L)$$

$$- e^{-9\pi/4}(\sin 3\pi w/2L - \cos 3\pi w/2L) + \cdots). \tag{38}$$

Using $w = u + iv$ and defining the symbols

$$\text{sc}[u, v] = \sin(\pi u/L)\cosh(\pi v/L)$$

$$\text{cs}[u, v] = \cos(\pi u/L)\sinh(\pi v/L) \tag{39}$$

and similar expressions for $\text{ss}[u, v]$ and $\text{cc}[u, v]$ which enable a compact notation for $\sin\pi w/L = \text{sc}[u, v] + i\,\text{cs}[u, v]$, the expression of $\zeta(w)$ in equation (23) is given in terms of trigonometric functions:

$$|\theta_1(w/L)| = 2q[(\text{sc}[u, v] - q^8\text{sc}[3u, 3v])^2 + (\text{cs}[u, v] - q^8\text{cs}[3u, 3v])^2]^{1/2}$$

$$\left(\sum_{\nu=1}^{4}|\theta_\nu(w/2L)|\right)^2 = 2\left[1 + q\left(\text{sc}\left[\tfrac{u}{2}, \tfrac{v}{2}\right] + \text{cc}\left[\tfrac{u}{2}, \tfrac{v}{2}\right]\right) - q^9\left(\text{sc}\left[\tfrac{3u}{2}, \tfrac{3v}{2}\right] - \text{cc}\left[\tfrac{3u}{2}, \tfrac{3v}{2}\right]\right)\right]^2$$

$$+ 2\left[1 + q\left(\text{cs}\left[\tfrac{u}{2}, \tfrac{v}{2}\right] - \text{ss}\left[\tfrac{u}{2}, \tfrac{v}{2}\right]\right) - q^9\left(\text{cs}\left[\tfrac{3u}{2}, \tfrac{3v}{2}\right] + \text{ss}\left[\tfrac{3u}{2}, \tfrac{3v}{2}\right]\right)\right]^2. \tag{40}$$

---

[6] The numerical value of the transition temperature has been deduced from different approaches, e.g. high-temperature series expansions (e.g. in [31]), temperature dependence of the correlation length (e.g. in [23]), zeros of the partition function (e.g. in [29]), jump in the helicity modulus (e.g. in [20]), ... and the recent estimations are compatible with each other.
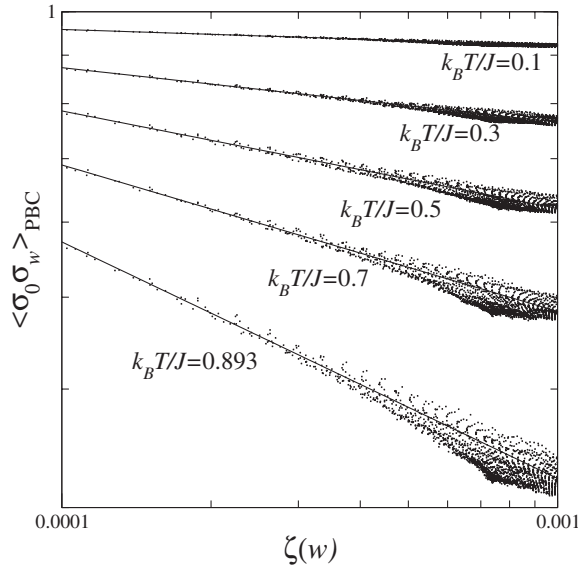
Figure 4. Log–log plot of the order parameter correlation function in a square system with periodic boundary conditions versus the rescaled variable $\zeta(w)$. The data correspond to a quarter of the lattice Λ, for $0 < u \leqslant L/2$ and $0 < v \leqslant L/2$, $L = 100$. Four different temperatures in the spin-wave phase are shown ($k_B T/J = 0.1$, 0.3, 0.5 and 0.7 from top to bottom), and at the KT transition temperature.

It is instructive to recover the cylinder limit from the torus geometry. For a square of arbitrary aspect ratio L'/L, the expansion parameter q in the previous series expansions has to be replaced by $e^{-\pi L'/L}$, and the larger the aspect ratio, the faster the series converges. Let us consider the limit $L' \to \infty$, L fixed. Keeping only the leading terms and omitting unimportant prefactors, we have

$$|\theta_1(w/L)| \underset{L'/L \to \infty}{\sim} |sc^2[u, v] + cs^2[u, v]|^{1/2} \tag{41}$$

hence from $\zeta(w) \sim |\theta_1(w/L)|$ the traditional expression [66] follows

$$\langle \boldsymbol{\sigma}_0 \cdot \boldsymbol{\sigma}_w \rangle_{\mathrm{PBC}} \sim \left[\cosh\left(\frac{2\pi v}{L}\right) - \cos\left(\frac{2\pi u}{L}\right) \right]^{-\frac{1}{2}\eta_\sigma} \tag{42}$$

which leads to equation (14) in the limit $v/L \gg 1$.[7]

We can then plot the correlation function data directly versus the rescaled variable $\zeta(w)$ on a log–log scale, as shown in figure 4. On this scale, a linear behaviour would indicate a power-law decay. A deviation from the straight line can be observed at large values of $\zeta(w)$ where the data are scattered. The quality of the data is unfortunately not improved by a better statistics (ten times more iterations). This correction is more pronounced as the KT point is approached where one knows that logarithmic corrections are present. From this figure, it is clearly difficult to get a reliable estimation of the exponents, but we nevertheless performed a fit in the range $\zeta(w) < 4 \times 10^{-4}$ where the behaviour is closer to a pure power law.[8]

---

[7] In the standard notation, the roles of u and v are reversed, because we have considered here the infinite direction of the cylinder in the imaginary direction.

[8] This range does not correspond to the right limit for an investigation of the asymptotic behaviour of the correlation function (especially when logarithmic corrections may be involved), since the limit $|z| \to \infty$ in the plane corresponds to $\zeta(w) \to \infty$.

Table 1. Values of the exponents of the bulk and surface correlation function in the spin-wave phase of the 2d XY model. They are obtained after fitting the density profiles or correlation functions to the conformal functional expressions for a system of size $L = 100$. We have checked that the results are already very stable at such a size. We mention that determinations a, b and c are completely independent for the bulk exponent, and that determinations d and e for the surface exponent are also independent. For determination e, the value of the bulk exponent in a is used as input. The most reliable results are printed in bold font.

| | Correlation function exponents | | | | | | |
| | η_σ | | | | $\eta_\parallel$ | | |
T	a	b	c	SW[a]	d	e	SW
0.1	0.017	**0.017(2)**	**0.017(1)**	0.016	**0.032(1)**	0.031	0.032
0.2	0.037	**0.035(4)**	**0.036(3)**	0.032	**0.069(1)**	0.064	0.064
0.3	0.057	**0.052(7)**	**0.052(5)**	0.048	**0.103(2)**	0.100	0.095
0.4	0.077	**0.073(9)**	**0.074(6)**	0.064	**0.143(4)**	0.140	0.127
0.5	0.103	**0.096(11)**	**0.100(8)**	–	**0.186(5)**	0.181	–
0.6	0.127	**0.122(14)**	**0.122(13)**	–	**0.231(8)**	0.228	–
0.7	0.154	**0.153(18)**	**0.155(14)**	–	**0.298(12)**	0.294	–
0.8	0.194	**0.188(22)**	**0.187(29)**	–	**0.374(17)**	0.366	–
0.893	0.249	**0.250(28)**	**0.250(34)**	–	**0.542(22)**	0.548	–

a Deduced from the fits of $\langle \boldsymbol{\sigma}_0 \cdot \boldsymbol{\sigma}_w \rangle_{\mathrm{PBC}}$ ($L = 100$), section 3.2.1.
b Deduced from the fits of $m_{\mathrm{FBC}}(w)$, section 3.3.1.
c Deduced from the fits of $m_{\mathrm{FfBC}}(w)$ ($L = 100$ or 200 at the KT point), section 3.3.2.
d Deduced from the fits of $m_{\mathrm{FfBC}}(w)$ ($L = 100$ or 200 at the KT point), section 3.3.2.
e Deduced from the fits of $\langle \boldsymbol{\sigma}_{w_1} \cdot \boldsymbol{\sigma}_w \rangle_{\mathrm{fBC}}$ ($L = 101$), section 3.2.2.
[a] SW gives the result of the spin-wave contribution.

The straight lines reported there correspond to (power-law fits with) slopes $\eta_\sigma(T)$ as given in table 1. They match perfectly the correlation function data in the regime of small $\zeta(w)$, therefore if they do not confirm nicely the expression in (24), they at least do not contradict this equation. A stronger support to equation (24) is the fact that the values of the exponents reported in table 1 are consistent with more refined estimates deduced from the fit of the order parameter profile in section 3.3 (the reader can compare columns a and b in table 1 to convince himself of the compatibility of the results).

3.2.2. Scaling of $\langle \boldsymbol{\sigma}_0 \cdot \boldsymbol{\sigma}_w \rangle_{\mathrm{fBC}}$. Simulations are then performed according to a similar procedure, but now in an open square with free BC along the four edges. Equation (28) may be used to estimate the surface exponent $\eta_\parallel(T)$. Plotting the quantity

$$\left\langle \boldsymbol{\sigma}_{w_1} \cdot \boldsymbol{\sigma}_w \right\rangle_{\mathrm{fBC}} \times [\kappa(w)]^{\frac{1}{2}\eta_\sigma(T)} = \psi(\omega) \tag{43}$$

as a function of the variable ω defined in equation (17), and given in terms of the w-coordinates as follows:

$$\omega = \mathrm{Im}\left[\mathrm{sn}\, \frac{2Kw_1}{L} \right] \times \mathrm{Im}\left[\mathrm{sn}\, \frac{2Kw}{L} \right] \times \left| \mathrm{sn}\, \frac{2Kw_1}{L} - \mathrm{sn}\, \frac{2Kw}{L} \right|^{-2} \tag{44}$$

will give access to the universal function $\psi(\omega)$. Here, the values of $\eta_\sigma(T)$ are taken from the previous section (column a in table 1). As we already mentioned above, these are not our most precise determinations of the bulk scaling dimensions, but the deviation from the forthcoming results of the following section being small (see table 1), there is no dramatic consequence to using them.
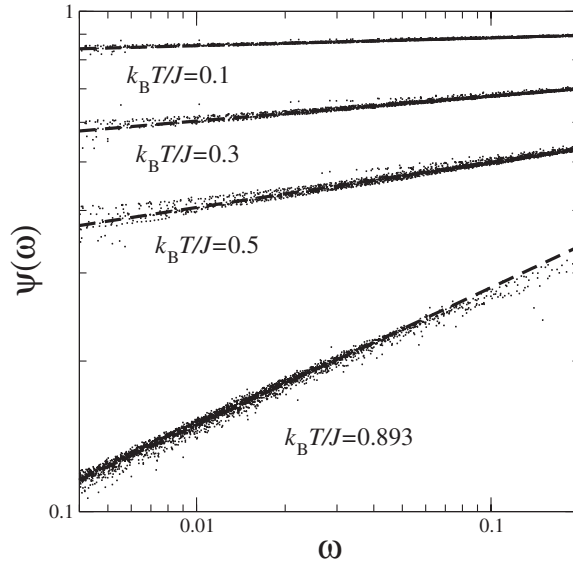
Figure 5. Log–log plot of the universal scaling function $\psi(\omega)$ at the KT point and below. The dashed lines represent a fit leading to the surface correlation function exponents ($L = 101$).

The function $\psi(\omega)$ is expected to behave as

$$\psi(\omega) \underset{\omega \ll 1}{\sim} \omega^{\frac{1}{2}\eta_\parallel(T)} \tag{45}$$

and leads to a determination of the surface exponent as a function of the temperature. In the case of the 2d Ising model for example, the scaling function was calculated analytically by Cardy [39],

$$\psi_{\text{Ising}}(\omega) = \sqrt{(1 + 4\omega)^{1/4} + (1 + 4\omega)^{-1/4}} \sim \omega^{1/2}\left(1 - \omega + \tfrac{9}{4}\omega^2 + \cdots\right) \tag{46}$$

in accordance with $\eta_\parallel^{\text{Ising}} = 1$.

The rescaled space variables $\kappa(w)$ and ω involve Jacobi elliptic sine. The series expansion is the following,

$$\text{sn}\,\frac{2Kw}{L} = \frac{2\pi}{kK} \sum_{n=0}^{\infty} \frac{e^{-\pi(n+1/2)}}{1 - e^{-\pi(2n+1)}} \sin\left[\frac{(2n+1)\pi w}{L}\right] \tag{47}$$

and the plot of $\psi(\omega)$ is shown in figure 5 at several temperatures below and at the KT transition. The surface scaling dimension $\frac{1}{2}\eta_\parallel(T)$ is deduced from a power-law fit at small values of $\omega \leqslant 0.03$ (dashed lines)[9]. At the Kosterlitz–Thouless transition, we can also fit the scaling function for comparison with the Ising case. One obtains

$$\psi_{\text{KT}}(\omega) \sim \omega^{0.274}(1 - 0.401\omega + 0.221\omega^2 + \cdots). \tag{48}$$

3.3. Behaviour of the density profiles

3.3.1. Scaling of $m_{\text{fBC}}(w)$.
Density profiles present the advantage of being one-point functions. They are thus supposed to be determined more precisely numerically than two-point correlation functions and should therefore lead to more refined estimations of the critical

---

[9] This is the right limit this time, since $|z| \to \infty$ corresponds to $\omega \to 0$.
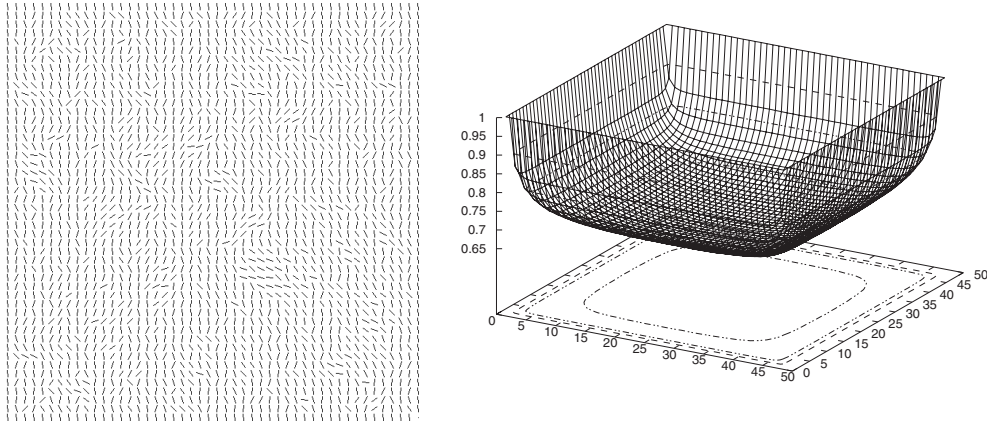
Figure 6. Monte Carlo simulations of the 2d *XY* model inside a square 48 × 48 spins with fixed boundary conditions below the Kosterlitz–Thouless transition temperature. Typical configuration on the left (where the fixed BC are easily observed by the common direction taken by all the border spins) and average over 10^6 MCS/spin after cancellation of 10^6 for thermalization (cluster update algorithm) on the right.

exponents. We start with simulations inside an open square with fixed boundary conditions (FBC), according to the prescriptions given in the description of the algorithm. The order parameter profile $m_{\text{FBC}}(w)$ is defined according to the definition of a reference orientation on the fixed boundaries, i.e.

$$m_{\text{FBC}}(w) = \langle \boldsymbol{\sigma}_w \cdot \boldsymbol{\sigma}_{\partial \Lambda(w)} \rangle_{\text{FBC}}$$
$$= \langle \cos(\theta_w - \theta_{\partial \Lambda(w)}) \rangle_{\text{FBC}}. \tag{49}$$

After averaging over the 'production sweeps', one gets a characteristic smooth profile as shown in figure 6 which also presents a typical configuration with fixed BC.

A log–log plot of $m_{\text{FBC}}(w)$ with respect to the reduced variable $\kappa(w)$ is shown in figure 7 at two different temperatures below T_{KT}, roughly at T_{KT}, and one temperature slightly above. A first observation is the confirmation of the functional form of equation (30) in the whole low-temperature phase. One indeed observes a very good data collapse of the L^2 points onto a single power-law master curve (a straight line on this scale). The next information is the rough confirmation of the value of the critical temperature, since above T_{KT}, the master curve is no longer a straight line, indicating that the corresponding decay in the half-infinite geometry differs from a power-law as it should in the high-temperature phase[10]. In [36], we have shown how the computation of the χ^2 per d.o.f. as a function of temperature is an indicator of the location of the KT transition. The χ^2 has a very small value, revealing the high quality of the fit, in the low-temperature phase and then increases significantly above T_{KT} when the behaviour of the density profile is no longer algebraic.

We have also shown that there is probably no logarithmic correction at the Kosterlitz–Thouless point, since the curve of figure 7 does not seem to differ significantly from a true power law. Although not a proof, numerical evidence of that is the plot of $m_{\text{FBC}}(w) \times [\kappa(w)]^{1/8}$ versus $\kappa(w)$ which remains constant on the whole range of values of $\kappa(w)$ [36]. This observation makes the order parameter profile with fixed boundary conditions a very convenient quantity for

[10] One should nevertheless mention that this does not lead to a precise determination of T_{KT}, since at $k_B T/J = 0.9$, for example, the master curve is hardly distinguishable from a straight line.
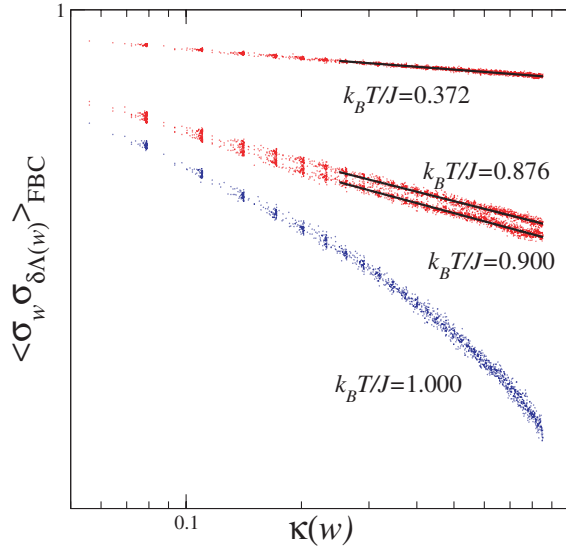
Figure 7. Monte Carlo simulations of the 2d *XY* model inside a square 100×100 spins (10^6 MCS/spin after cancellation of 10^6 for thermalization, cluster update algorithm). The figure shows the rescaled order parameter density against the rescaled distance on a log–log scale at different temperatures below the Kosterlitz–Thouless transition temperature and slightly above.

the determination of the bulk correlation function exponent, since it displays a pure algebraic decay up to the Kosterlitz–Thouless transition point[11].

Fitting the curves of figure 7 to power laws leads to the values of the scaling dimension $\eta_\sigma(T)$ in the whole critical region $T \leqslant T_{KT}$ as shown in figure 10 in the conclusion. The data are also reported in table 1. The accuracy is much better than in the case of the two-point correlation functions.

3.3.2. Scaling of $m_{FfBC}(w)$. For this last choice of boundary conditions, hereafter referred to as 'fixed–free BC' (and denoted by FfBC), the open square has half of its boundaries which are left free while the other half are kept fixed. This is illustrated in figure 8 where the averaged profile is also shown at two different temperatures. The shape of the plotted surface helps in understanding the BC.

In the previous section, we reported some evidence that the logarithmic corrections at the KT point are negligible for the order parameter profile with fixed BC. Assuming that there will be no substantial difference for fixed–free BC, we perform a fit of $\ln m_{FfBC}(w)$ against the two-dimensional linear expression, $\text{const} - \frac{1}{2}\eta_\sigma(T)\ln\kappa(w) + \frac{1}{2}\eta_\parallel(T)\ln\mu(w)$, as expected from equation (34). The value obtained for the bulk correlation function exponent $\eta_\sigma(T)$ (already known precisely from the previous section) will be a test for the reliability of the fit. The simulations are performed at several temperatures, up to $k_B T_{KT}/J \simeq 0.893$. The three parameters linear fits lead to correct determinations of both exponents (we studied different system sizes ranging between $L = 48$ and $L = 100$ and even 200 at the KT point). The value of the bulk exponent is in good agreement with the determination which follows from the fit

---

[11] The decay exponent, if not fixed, but determined numerically, leads to a quite good result (for example, for a size $L = 100$, we get $\eta_\sigma(T_{KT}) = 0.250(28)$).

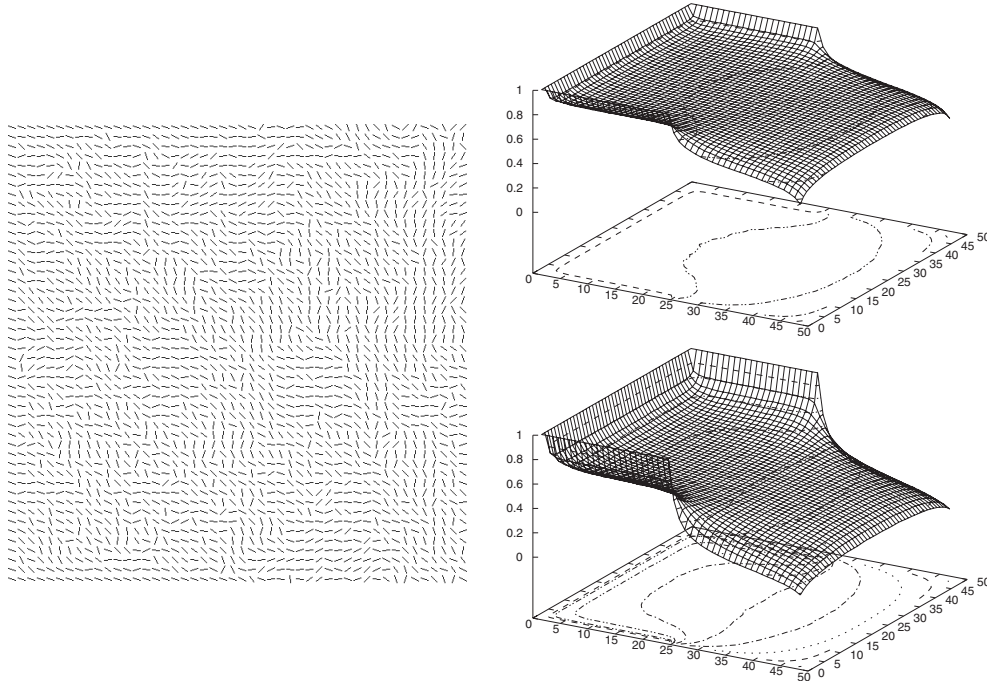**Figure 8.** Monte Carlo simulations of the 2d *XY* model inside a square 48×48 spins with mixed fixed–free boundary conditions below the Kosterlitz–Thouless transition temperature. Typical configuration on the left and average over 10^6 MCS/spin after cancellation of 10^6 for thermalization (cluster update algorithm) at $k_B T/J = 0.488$ and $k_B T/J = 0.915$ on the right.

of the profile with fixed BC, and the surface exponent also fits nicely to the values deduced from the two-point correlation function with free BC.

3.3.3. Scaling of $\Delta \varepsilon_{\text{FBC}-\text{fBC}}(w)$. We concentrated mainly up to now on the magnetic properties. The thermal exponents are also interesting quantities which characterize a critical point. In the case of the *XY* model, the temperature is a marginal field, responsible for the existence of a critical line in the whole low-temperature phase. It thus implies a thermal scaling exponent $x_\varepsilon = d - y_t = 2$ which ensures a vanishing RG eigenvalue $y_t = 0$ (up to T_{KT} where it is consistent with the essential singularity of ξ above the KT point). The energy–energy correlation function should thus decay algebraically as

$$\left\langle \varepsilon_{z_1} \varepsilon_{z_2} \right\rangle \sim |z_1 - z_2|^{-\eta_\varepsilon} \tag{50}$$

with $\eta_\varepsilon(T) = 2x_\varepsilon = 4, \forall T < T_{\text{KT}}$.

We check qualitatively this expression of the energy–energy correlations from the behaviour of the energy density profile. The energy density at site w is, for example, defined as the average value of the energies of the four links reaching w:

$$\varepsilon_w = \frac{1}{2d} \sum_{\hat{\mu}} (\boldsymbol{\sigma}_{w-\hat{\mu}} \cdot \boldsymbol{\sigma}_w + \boldsymbol{\sigma}_w \cdot \boldsymbol{\sigma}_{w+\hat{\mu}}). \tag{51}$$

In comparison with the magnetization profile, a difficulty occurs due to the existence of a regular contribution in the energy density. This term cancels after a suitable difference between profiles obtained with different BC. For that reason, we made two different series of
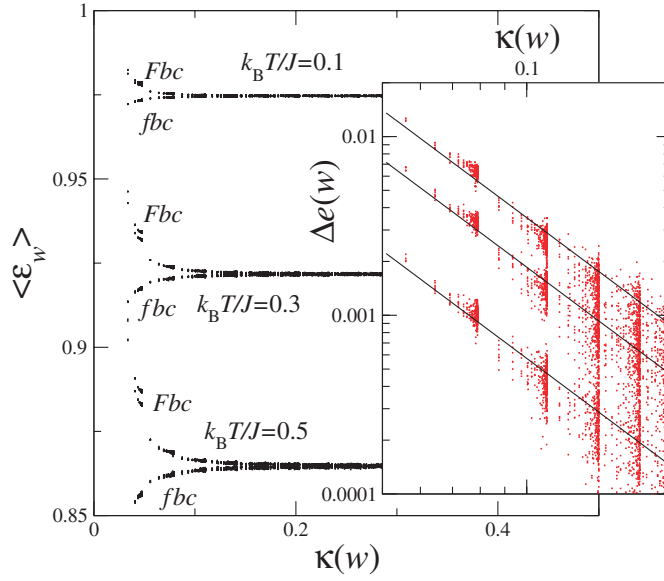
Figure 9. Monte Carlo simulations of the 2d *XY* model inside a square 100×100 spins (10^6 MCS/spin after cancellation of 10^7 for thermalization, cluster update algorithm). The main figure shows the local energy density versus the rescaled variable $\kappa(w)$ at different temperatures and for different BC. The inset is a log–log plot of the difference $\Delta e(w)$ as explained in the text.

simulations with free (fBC) and fixed (FBC) boundary conditions. From the latter simulations we had already extracted the singular behaviour of the magnetization profile since there is no regular contribution in the scale-invariant phase,

$$m_{\text{FBC}}(z) = \mathcal{A}_m(T) y^{-\eta_\sigma(T)/2} \tag{52}$$

where $\mathcal{A}_m(T)$ is a non-universal 'critical' amplitude[12] which depends on the temperature.

On the other hand, the two series of simulations are necessary in order to extract the singularity associated with the energy density which contains a non-universal regular contribution $\langle \varepsilon_0(T) \rangle$ which depends on T and a singular contribution:

$$\langle \varepsilon_z \rangle_{\text{FBC}} = \langle \varepsilon_0(T) \rangle + \mathcal{B}_{\text{FBC}}(T) y^{-\eta_\varepsilon(T)/2} \tag{53}$$

$$\langle \varepsilon_z \rangle_{\text{fBC}} = \langle \varepsilon_0(T) \rangle + \mathcal{B}_{\text{fBC}}(T) y^{-\eta_\varepsilon(T)/2}. \tag{54}$$

This is clearly illustrated in figure 9 where convergence towards the same temperature-dependent constant $\langle \varepsilon_0(T) \rangle$ is shown. We also observe that the amplitudes of the singular terms have opposite signs. Therefore, a simple difference of the quantities measured in the square geometry,

$$\Delta e(w) = \langle \varepsilon_w \rangle_{\text{FBC}} - \langle \varepsilon_w \rangle_{\text{fBC}} \sim \Delta \mathcal{B} \times [\kappa(w)]^{-\frac{1}{2}\eta_\varepsilon(T)} \tag{55}$$

leads to the value of the thermal scaling dimension $\eta_\varepsilon(T)$.

The inset in figure 9 shows a log–log plot of the difference $\Delta e(w)$ versus $\kappa(w)$ at three temperatures below T_{KT}. Due to strong fluctuations, the data scatter around straight lines which represent the theoretical slopes $[\kappa(w)]^{-2}$. This figure, though far from being definitely conclusive, confirms that the exponent of the decay of energy–energy correlations keeps a

---

[12] Here we use the term 'critical', since the whole low-temperature phase is considered as critical.
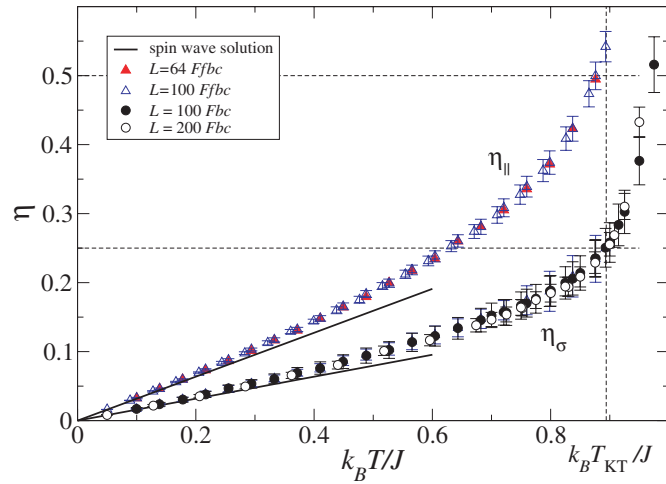
Figure 10. Bulk and surface correlation decay exponents of the 2d *XY* model as a function of the temperature. The values follow from independent linear fits of the magnetization profiles with F$_{BC}$ (circles) or Ff$_{BC}$ (triangles).

constant value $\eta_\varepsilon(T) = 4$ in the low-temperature phase of the *XY* model. At the KT transition, this value was confirmed very accurately by Blöte and Nienhuis [56].

4. Discussion

The different determinations of the bulk and surface correlation function scaling dimensions reported in this paper are mutually consistent. These exponents are obtained using completely independent techniques, from four independent series of simulations (the boundary conditions, but also the quantities which are computed are different). The fits themselves are different, since these quantities obey specific functional expressions.

The exponents are plotted in figure 10 for different system sizes. Our results (for a few values of the temperature) are also given in table 1. In columns *a*, *b* and *c* we present the bulk exponent. Columns *d* and *e* give the surface exponent. The error bars (for the values resulting from the fits of the magnetization profiles, columns *b*, *c*, *d*) correspond to one standard deviation. We have to mention here that these error bars should be considered with some care for at least two reasons. A first reason is that we did not make any extrapolation to the thermodynamic limit, because the results at a few sizes already seem very stable as can be observed in figure 10. Although we did not analyse the size effects systematically, we believe that this is not the most important contribution to the error. A second reason has more drastic consequences. This is the influence of the fitting window. When the range of fit is varied in a *reasonable* scale in the 'large κ' regime, it usually produces a small deviation in the resulting exponent. For example, fitting a power law $\sim[\kappa(w)]^x$ in the window $0.10 < \kappa(w) < 1$ or $0.25 < \kappa(w) < 1$ leads to compatible results within the error bars (in this example at the KT transition, we get respectively $\eta_\sigma = 0.260(18)$ and $0.250(28)$). If the window range is changed significantly, on the other hand, we no longer control the stability of the results, since the errors increase considerably (for example, $\eta_\sigma = 0.247(92)$ for $0.50 < \kappa(w) < 1$). Because of these constraints, we believe that the values of the exponents that we measure are reliable, but the errors are only rough estimates.

The weaker result of the paper probably comes from the correlation function with periodic boundary conditions which is fitted to an approximate functional expression. There are also logarithmic corrections in this case and an unavoidable scattering of the data which prevent a fit in the interesting asymptotic region. The consequence is a bulk exponent which is *a priori* obtained with a poor level of confidence, and for this reason we decided to avoid any error bar in column *a* of table 1. It is amazing to observe that in spite of these restrictions, these results do indeed agree with the most refined values deduced from the magnetization density profile with fixed boundary conditions (see column *b* in table 1). Another consequence of our approach is again the *a priori* weak level of confidence of the surface exponent deduced from the correlations in the open system (column *e* in the table), since we use the bulk values from column *a* as input parameters for this latter fit. The surface exponent in fact fits correctly the most refined values deduced from the magnetization density profile with mixed fixed–free boundary conditions (column *d*). Obviously, the stronger results come from the magnetization profile analyses. We believe also that another result of interest is the confirmation that the functional expressions derived in section 2 are valid and are in fact very efficient for the numerical investigation of critical properties of two-dimensional systems. Such applications of conformal mappings are, of course, well known in the case of strip geometries with, e.g., the celebrated correlation length–amplitude-exponent relation [65].

Let us now briefly discuss the results. In the low-temperature limit, one knows that the spin-wave description captures the essential of the physics of the problem. From this limit, the linear behaviour of the bulk exponent with the temperature, $\eta_\sigma(T) = k_B T / 2\pi J$, is easily recovered. It is, of course, reasonable to expect that the low-temperature limit of the surface exponent can also be recovered by the spin-wave approximation (see the appendix). Indeed, the surface properties of the Gaussian model at the ordinary transition were studied by Cardy [39]. They describe the low-temperature regime of the *XY* model. The surface–bulk correlation function exhibits an algebraic decay

$$\langle \cos(\theta_0 - \theta_{\mathbf{r}}) \rangle_{\text{UHP}} \simeq \left(\frac{\pi r}{a} \right)^{-1/\pi K} \tag{56}$$

and the corresponding surface exponent is thus given in the spin-wave approximation by the linear behaviour

$$\eta_\parallel(T) = \frac{k_B T}{\pi J} \qquad T \to 0. \tag{57}$$

This result is simply twice the bulk value, $\eta_\parallel(T) = 2\eta_\sigma(T)$. This relation fits the numerical data at low temperature as shown in figure 10 or in the table.

At the KT transition, the bulk exponent is fully coherent with the result of Kosterlitz and Thouless RG analysis $\eta_\sigma(T_{\text{KT}}) = 1/4$. For the surface, the value $\eta_\parallel(T_{\text{KT}}) \simeq 0.54$ is close to the known result $\frac{1}{2}$ [39], a value which cannot be excluded from our analysis (though out of the error bar), since the uncertainties that we quote are only indications. It is also coherent with the surface exponent obtained at the KT point of the quantum Ashkin–Teller chain ($\epsilon = -2^{-1/2}$ in [66]), $\eta_\parallel(T_{\text{KT}}) = 2\pi^{-1} \arccos(-\epsilon) = 1/2$. This value is furthermore in agreement with the relation $\eta_\parallel(T) = 2\eta_\sigma(T)$, provided that it is valid up to the KT point. This relation was established in the spin-wave approach, and to extend it to the vortex-dominated regime, closer to T_{KT}, we note that the effect of vortices (when $T \to T_{\text{KT}}^-$) when treated in the Coulomb gas approach [13, 15] is only to increase the effective temperature in the spin-wave approximation, hence to enhance the decay of the correlations. Like $\eta_\parallel(T) = 2\eta_\sigma(T) = k_B T / \pi J$ is correct in the spin-wave treatment, the relation $\eta_\parallel(T_{\text{eff}}) = 2\eta_\sigma(T_{\text{eff}}) = k_B T_{\text{eff}} / \pi J$ should hold in the whole critical phase, with a shift in temperature which depends on the vortice interactions,

$$k_B T_{\text{eff}} = k_B T - \frac{1}{2} \pi^2 \sum_{|\mathbf{r}| > a} r^2 \langle q(0) q(\mathbf{r}) \rangle \tag{58}$$
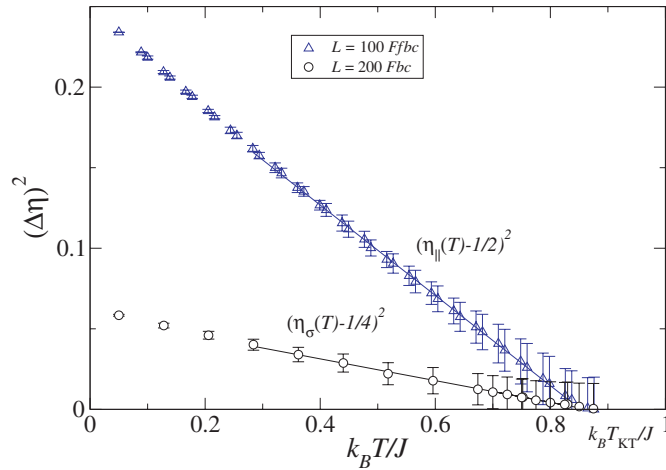
Figure 11. Square root behaviour of the bulk and surface correlation function exponents as the Kosterlitz–Thouless point is approached.

where $\langle q(0)q(\mathbf{r})\rangle$ are the vortex intensity correlations (which are negative in the neutral low-temperature phase). It is thus reasonable to expect that the relation $\eta_\parallel(T) = 2\eta_\sigma(T)$ is exact for the whole critical phase of the model. It can be checked that the numerical values in table 1 support this expression.

The approach of the KT point, where the temperature dependence of the bulk correlation function exponent is known, is also interesting. From the numerical data, $\eta_\sigma(T)$ can be expanded close to the KT point $T \to T_{\mathrm{KT}}^-$, showing a leading square root behaviour [14, 23] as illustrated in figure 11. The same behaviour is obtained for the surface exponent. One should nevertheless mention here that the plot of $\left(\eta_\sigma(T) - \frac{1}{4}\right)^2$ or $\left(\eta_\parallel(T) - \frac{1}{2}\right)^2$ against T seems to indicate a slightly lower value of T_{KT} than 0.893. A clarification of that point is beyond the scope of this paper, since it would definitely require simulations of really large systems in order to rule out the possibility of finite-size dependence of the measured quantities.

Eventually, we mention that our analysis of the energy density profiles is compatible with the marginality condition of the temperature in the low-temperature phase of the *XY* model. This condition, equivalent to the continuous variation of the magnetic scaling dimension, indeed implies that the thermal scaling dimension keeps a constant value $x_\varepsilon = 2$ which does not depend on the temperature, and this value enables the numerical data to fitted reasonably.

In this paper, we performed an accurate study of the low-temperature phase of the 2d *XY* model using efficient techniques, based on a conformal mapping of the correlation functions and density profiles. At the Kosterlitz–Thouless transition, the results are in agreement with the general picture of the RG analysis and the critical exponents describing the algebraic decay of the correlations in the low-temperature phase are measured.

Acknowledgments

Note added in proof.   I gratefully acknowledge L N Shchur who drew my attention to a recent paper where similar results were reported [67].

Appendix

In this appendix, we recall the surface–bulk correlation function obtained in the spin-wave approximation. The correlation function between a spin close to the surface (σ_0) and another spin far into the bulk (σ_z) is defined according to $\langle \sigma_0 \cdot \sigma_z \rangle_{\text{UHP}} = \langle \cos(\theta_0 - \theta_z) \rangle_{\text{UHP}}$, where the subscript UHP means here that $\text{Im}\, z \geqslant 0$. We use a standard notation $\mathbf{r}$ for z from now on. As is well known, in the harmonic approximation, the Hamiltonian becomes quadratic and the thermal average leads to the Gaussian model which implies that

$$\langle \cos(\theta_0 - \theta_{\mathbf{r}}) \rangle_{\text{UHP}} = \exp\left(-\tfrac{1}{2}\langle (\theta_0 - \theta_{\mathbf{r}})^2 \rangle_{\text{UHP}}\right). \tag{A.1}$$

In Fourier space, $\theta_{\mathbf{r}} = N^{-1/2} \sum_{\mathbf{q}} \exp(-i\mathbf{q}\mathbf{r})\theta_{\mathbf{q}}$ ($N = L^2$), the Hamiltonian becomes (the spins are located on the vertices of a square lattice of spacing unit a)[13]

$$-\frac{H}{k_B T} \simeq \text{const} - \frac{1}{4}K \sum_{\mathbf{q}} 2(2 - \cos aq_x - \cos aq_y)|\theta_{\mathbf{q}}|^2$$

$$\simeq \text{const} - \frac{1}{4}K \sum_{\mathbf{q}} a^2 |\mathbf{q}|^2 |\theta_{\mathbf{q}}|^2 \tag{A.2}$$

and leads to a partition function

$$Z_\beta = \prod_{\mathbf{q}} \left(\frac{4\pi}{Ka^2|\mathbf{q}|^2}\right)^{1/2}. \tag{A.3}$$

Hence, the quadratic fluctuations of the Fourier amplitudes are linear in T,

$$\langle |\theta_{\mathbf{q}}|^2 \rangle = \frac{2}{Ka^2|\mathbf{q}|^2} \tag{A.4}$$

and the integral $\left(N^{-1} \sum_{\mathbf{q}} \to \frac{a^2}{4\pi^2} \int d\mathbf{q}\right)$

$$\langle (\theta_0 - \theta_{\mathbf{r}})^2 \rangle = \frac{a^2}{2\pi^2} \int d\mathbf{q}(1 - \cos \mathbf{q}\mathbf{r})\langle |\theta_{\mathbf{q}}|^2 \rangle \tag{A.5}$$

is easily evaluated, leading to

$$\langle (\theta_0 - \theta_{\mathbf{r}})^2 \rangle = \frac{1}{\pi^2 K} \int_0^{2\pi} \frac{dq}{q} \int_0^{\pi} d\varphi(1 - \cos qr \cos \varphi)$$

$$= \frac{1}{\pi K} \int_0^{\pi r/a} \frac{1 - J_0(u)}{u}\, du$$

$$\simeq \frac{1}{\pi K} \ln \frac{\pi r}{a} \tag{A.6}$$

where a cutoff $\sim \pi/a$ was introduced. The surface–bulk correlation function follows:

$$\langle \cos(\theta_0 - \theta_{\mathbf{r}}) \rangle_{\text{UHP}} \simeq \left(\frac{\pi r}{a}\right)^{-1/\pi K} \tag{A.7}$$

and the corresponding surface exponent is thus given in the spin-wave approximation by the linear behaviour

$$\eta_{\parallel}(T) = \frac{k_B T}{\pi J} \qquad T \to 0. \tag{A.8}$$

---

[13] In contrast with the standard calculation in the whole plane, an extra factor of $1/2$ appears from the orthogonality relation in the UHP.

References

[1] Nelson D R 2002 *Defects and Geometry in Condensed Matter Physics* (Cambridge: Cambridge University Press)
[2] Hasenbusch M and Török T 1999 *J. Phys. A: Math. Gen.* **32** 6361
[3] Mermin N D and Wagner H 1966 *Phys. Rev. Lett.* **22** 1133
[4] Hohenberg P C 1967 *Phys. Rev.* **158** 383
[5] Berezinskii V L 1971 *Sov. Phys.–JETP* **32** 493
[6] Stanley H E and Kaplan T A 1966 *Phys. Rev. Lett.* **17** 913
[7] Rice T M 1965 *Phys. Rev.* A **140** 1889
[8] Wegner F 1967 *Z. Phys.* **206** 465
[9] Sarma G 1972 *Solid State Commun.* **10** 1049
[10] Tsallis C 1976 *Nuovo Cimento* **34** 411
[11] Kosterlitz J M and Thouless D J 1973 *J. Phys. C: Solid State Phys.* **6** 1181
[12] Kosterlitz J M 1974 *J. Phys. C: Solid State Phys.* **7** 1046
[13] Villain J 1975 *J. Phys.* **36** 581
[14] Kosterlitz J M and Thouless D J 1978 *Prog. Low Temp. Phys.* **78** 371
[15] Itzykson C and Drouffe J M 1989 *Statistical Field Theory* vol 1 (Cambridge: Cambridge University Press)
[16] Cardy J L 1996 *Scaling and Renormalization in Statistical Physics* (Cambridge: Cambridge University Press)
[17] Gulácsi Z and Gulácsi M 1998 *Adv. Phys.* **47** 1
[18] Fernández J F, Ferreira M F and Stankiewicz J 1986 *Phys. Rev.* B **34** 292
[19] Gupta R, DeLapp J, Batrouni G G, Fox G C, Baillie C F and Apostolakis J 1988 *Phys. Rev. Lett.* **61** 1996
[20] Weber H and Minnhagen P 1988 *Phys. Rev.* B **37** 5986
[21] Bifferale L and Petronzio R 1989 *Nucl. Phys.* B **328** 677
[22] Wolff U 1989 *Nucl. Phys.* B **322** 759
[23] Gupta R and Baillie C F 1992 *Phys. Rev.* B **45** 2883
[24] Janke W and Nather K 1993 *Phys. Rev.* B **48** 7419
[25] Olsson P 1995 *Phys. Rev.* B **52** 4526
[26] Kenna R and Irving A C 1995 *Phys. Lett.* B **351** 273
[27] Kim J K 1996 *Phys. Lett.* A **223** 261
[28] Janke W 1997 *Phys. Rev.* B **55** 3580
[29] Kenna R and Irving A C 1997 *Nucl. Phys.* B **485** 583
[30] Butera P, Comi M and Marchesini G 1989 *Phys. Rev.* B **40** 534
[31] Butera P and Comi M 1994 *Phys. Rev.* B **50** 3052
[32] Amit D J, Goldschmidt Y Y and Grinstein G 1980 *J. Phys. A: Math. Gen.* **13** 585
[33] Zisook A B and Kadanoff L P 1980 *J. Phys. A: Math. Gen.* **13** L379
[34] Campostrini M, Pelissetto A, Rossi P and Vicari E 1996 *Phys. Rev.* B **54** 7301
[35] Van Himbergen J E 1984 *J. Phys. C: Solid State Phys.* **17** 5039
[36] Berche B, Fariñas Sanchez A I and Paredes V R 2002 *Europhys. Lett.* **60** 539
[37] Berche B 2002 *Phys. Lett.* A **302** 336
[38] Henkel M 1999 *Conformal Invariance and Critical Phenomena* (Heidelberg: Springer)
[39] Cardy J L 1984 *Nucl. Phys.* B **240** 514
[40] Itzykson C and Drouffe J-M 1989 *Théorie statistique des champs* vol 2 (Paris: InterEditions/Editions du CNRS) chapter IX
[41] Barber M N, Peschel I and Pearce P A 1984 *J. Stat. Phys.* **37** 497
[42] Davies B and Peschel I 1991 *J. Phys. A: Math. Gen.* **24** 1293
[43] Burkhardt T W and Eisenriegler E 1986 *J. Phys. A: Math. Gen.* **19** L663
[44] Burkhardt T W and Xue T 1991 *Phys. Rev. Lett.* **66** 895
[45] Burkhardt T W and Xue T 1991 *Nucl. Phys.* B **354** 653
[46] Turban L and Iglói F 1997 *J. Phys. A: Math. Gen.* **30** L105
[47] Burkhardt T W and Derrida B 1985 *Phys. Rev.* B **32** 7273
[48] Kleban P, Akinci G, Hemtschke R and Brownstein K R 1986 *J. Phys. A: Math. Gen.* **19** 437
[49] Peschel I, Turban L and Iglói F 1991 *J. Phys. A: Math. Gen.* **24** L1229
[50] Blawid S and Peschel I 1994 *Z. Phys.* B **95** 73
[51] Berche B, Debierre J-M and Eckle H P 1994 *Phys. Rev.* E **50** 4542
[52] Iglói F, Peschel I and Turban L 1993 *Adv. Phys.* **42** 683
[53] di Francesco P, Saleur H and Zuber J-B 1987 *Nucl. Phys.* B **290** 527
[54] Talapov A L, Andreichenko V B, Dotsenko Vl S and Shchur L N 1993 *Int. J. Mod. Phys.* C **4** 787

[55] Talapov A L and Shchur L N 1994 *Europhys. Lett.* **27** 193
[56] Blöte H W J and Nienhuis B 1989 *J. Phys. A: Math. Gen.* **22** 1415
[57] Allton C R and Hamer C J 1988 *J. Phys. A: Math. Gen.* **21** 2417
[58] di Francesco P, Mathieu P and Sénéchal D 1997 *Conformal Field Theory* (New York: Springer) chapter 12
[59] Lavrentiev M and Chabat B 1972 *Méthodes de la théorie des fonctions d'une variable complexe* (Moscow: Mir) chapter VII
[60] Chatelain C and Berche B 1999 *Phys. Rev.* E **60** 3853
[61] Fisher M E and de Gennes P G 1978 *C. R. Acad. Sci., Paris* B **287** 207
[62] Carlon E and Iglói F 1998 *Phys. Rev.* B **57** 7877
[63] Wolff U 1989 *Phys. Rev. Lett.* **62** 361
[64] Abramowitz M and Stegun I A 1970 *Handbook of Mathematical Functions* (New York: Dover)
[65] Cardy J L 1987 *Phase Transitions and Critical Phenomena* ed C Domb and J L Lebowitz (London: Academic) p 55
[66] Carlon E, Lajkó P and Iglói F 2001 *Phys. Rev. Lett.* **87** 277201
[67] Reš I and Straley J 2000 *Phys. Rev.* B **61** 14425